Mechanics of 3-D shear cracks between Rayleigh and shear wave rupture speeds

Andrea Bizzarri [a,*], Shamita Das [b,1]

[a] Istituto Nazionale di Geofisica e Vulcanologia, Sezione di Bologna, Italy Via Donato Creti, 12-40128 Bologna, Italy
[b] University of Oxford, Department of Earth Sciences, South Parks Road, Oxford OX1 3AN, UK

ABSTRACT

Though mode II shear fractures (primarily strike-slip earthquakes) can not only exceed the shear wave speed of the medium, but can even reach the compressional wave speed, steady-state calculations showed that speeds between the Rayleigh and shear wave speeds were not possible, thus defining a forbidden zone. For more than 30 years it was believed that this result in which the rupture jumps over the forbidden zone, also holds for 3-D ruptures, in which mode II and mode III (mainly dip-slip faulting) are mixed. Using unprecedentedly fine spatial and temporal grids, we show that even in the simple configuration of homogeneous fault properties and linear slip-weakening friction law, a realistic 3-D rupture which starts from rest and accelerates to some higher velocity, actually does pass smoothly through this forbidden zone, but very fast. The energy flux from the rupture tip is always positive, even within the so-called forbidden zone, contrary to the 2-D case. Finally, our results show that the width of the cohesive zone initially decreases, then increases as the rupture exceeds the shear wave speed and finally again decreases as the rupture accelerates to a speed of $\sim$90% of the compressional wave speed.

© 2012 Elsevier B.V. All rights reserved.

1. Introduction

In 1955, Gutenberg studied the 1952 magnitude 7.6 Kern County, California earthquake and concluded that the rupture had progressed at a speed of about 90% of the shear wave speed of the medium (Gutenberg, 1995). Study of the great 1960 Chilean earthquake (Benioff et al., 1961) of magnitude 9.5 and the great 1952 Kamchatka earthquake of magnitude 9.0 (Ben-Menhahem and Toksöz, 1963) also led to similar results. Though these were dip-slip earthquakes (mainly anti-plane mode), it led to the belief that the maximum earthquake rupture speeds were limited by the Rayleigh wave speed (v_R). The idea was supported by fracture mechanics studies which showed that tension cracks and in-plane shear cracks also had this limiting speed, for very idealized theoretical perfectly brittle fracture models. In the early 1970's, theoretical studies using more realistic models showed that mode II cracks not only could exceed v_R but could even reach the compressional wave speed, v_P (about 70% higher than the shear wave speed v_S for Poisson solids) (Andrews, 1976; Das and Aki, 1977). Since the 1990's, this result has been confirmed by laboratory experiments (Rosakis et al., 1999) and several examples of strike-slip earthquakes reaching such speeds have been found (Bouchon et al.,

2001; Robinson et al., 2006). However, self-similar calculations, in which a 2-D, pure mode II crack suddenly appears and starts extending at a constant speed, showed that speeds between the Rayleigh and the shear wave speeds are not possible, based on energy considerations (Andrews, 1976; Burridge et al., 1979; Broberg, 1999). Andrews (1994), starting from Burridge (1973), founds self-similar solution in between v_R and v_S (non-spontaneous solutions, i.e., with prior assigned rupture speed), which are not physically realistic for pure mode II spontaneous ruptures and his solutions are singular at the crack tip. Moreover, his numerical calculations of a mixed-mode rupture (in which there are two non-null components of the solutions, but both depends only on a single spatial coordinate; see Bizzarri, 2011, his Section 2.1 for further details) has poor resolution and therefore cannot handle the question of the penetration of the "forbidden zone" properly.

In this paper we will explore whether for realistic cases where a crack starts from rest and accelerates spontaneously (the rupture speed is a part of the solution) to some higher speed, the rupture actually jumps over this "forbidden zone" or passes through it. This is important for earthquake engineering applications as it is the acceleration of the crack edge that controls the radiation of the waves which cause most damage (Madariaga, 1983). An additional motivation is that supershear earthquake ruptures could produce larger ground velocities, accelerations and stresses at some distances from the fault trace compared to subshear ones (Bernard and Baumont, 2005; Dunham and Archuleta, 2005; Bizzarri et al., 2010).

* Corresponding author. Tel.: +39 051 4151432; fax: +39 051 4151499.
  E-mail addresses: bizzarri@bo.ingv.it (A. Bizzarri), das@earth.ox.ac.uk (S. Das).
  [1] Tel.: +44 1 865 272015; fax: +44 1 865 272072.

2. Method

In this paper we deliberately consider the most simple, or canonical, configuration for faulting. Although large earthquakes generally occur on a complex interacting fault system rather than a single isolated structure, in order to better understand the supershear transition and compare the results with the theoretical predictions discussed in the main text, we model the spontaneous rupture propagation on a planar, vertical fault having homogeneous rheological properties and separating two isotropic, perfectly elastic media having identical properties and taken to be Poisson solids. A sketch of the fault model is showed in Fig. 1a. The rupture is truly 3-D, in that it is a mixture of mode II (in-plane shear) and mode III (anti-plane shear) propagation, each of which explicitly depends on the two on-fault coordinates x_1 and x_3 and rake rotation is allowed in our model. We do not allow any tensile component, so that the slip is continuous in the x_2-direction. Modes II and III constitute the most important

mechanisms for seismic wave excitation and generating ground shaking. The fundamental elastodynamic equation neglecting body forces is solved numerically, by adopting an OpenMP parallel, 2nd-order accurate, finite difference, conventional grid method, which is described in details in Bizzarri and Cocco (2005) and Bizzarri (2009).

At the initial instant, the medium is assumed to be in equilibrium and the initial shear stress on the fault is directed in the x_1-direction, defining a strike-slip mechanism. For sake of simplicity, we assume here that its magnitude τ_0 is homogeneous over the whole fault plane, defined by the two dimensions L^f and W^f in the strike and depth direction, respectively. We set both L^f and W^f in order to avoid that the arrest waves generated from the fault boundaries can stifle the supershear transition. By assuming homogeneous properties on the fault surface we intentionally neglect the complexity of the seismic radiation which emerges from the inhomogeneity of the stress drop distribution (e.g., Madariaga, 1983). The rupture starts from an imposed hypocenter
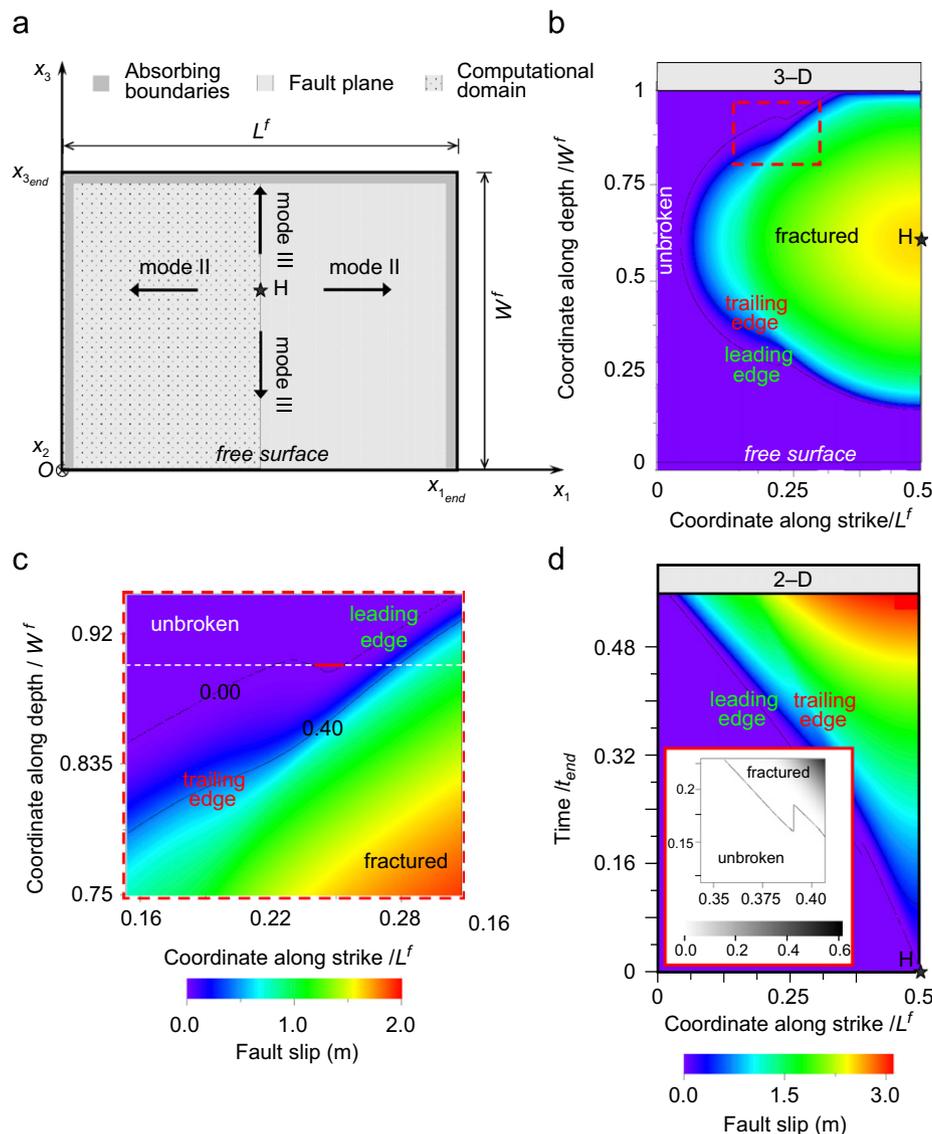

Fig. 1. (a) Geometry of the fault. The rupture starts from the hypocenter H and spreads out in all directions over a vertical plane, and the material properties are homogeneous (see Table 1). (b) Snapshot of the slip distribution on the left half of the fault plane for a 3-D rupture at the 62% of the total computational time (t_{end}=3.12 s). Dashed red lines show the portion of this figure which is shown expanded in (c). (d) Slip distribution for a 2-D pure mode II rupture (propagating along x_1), plotted against the strike coordinate and time. The fault properties are the same as for (a). The inset shows a zoom-in of the crack tip bifurcation. Contours defining the leading and trailing edges of the cohesive zone (region where the fault slip lies between 0 and the slip-weakening distance d_0) are shown in panels (b)–(d). (For interpretation of the references to color in this figure legend, the reader is referred to the web version of this article.)

Table 1
Parameters adopted in the present paper.

Parameter	Value
Medium and Discretization Parameters	
Lamé' s constants, $\lambda = G$	35.9 GPa
S wave velocity, v_S	3.464 km/s
Rayleigh velocity, v_R	3.184 km/s
P wave velocity, v_P	6 km/s
Eshelby velocity, $v_E = \sqrt{2}v_S$	4.899 km/s
Fault length, L^f	16 km
Fault width, W^f	12 km[a]
Spatial grid size, Δx	5 m[b]
Final time, t_{end}	3.12 s
Time step, Δt	1.2×10^{-4} s[c]
Coordinates of the hypocenter, $H \equiv (x_1^H, x_3^H)$	(8, 7) km
Fault Constitutive Parameters	
Magnitude of the effective normal stress, σ_n^{eff}	120 MPa
Magnitude of the initial shear stress (pre-stress), τ_0	73.8 MPa
Static friction coefficient, μ_u	0.677 ($\leftrightarrow \tau_u$=81.24 MPa)
Dynamic friction coefficient, μ_f	0.46 ($\leftrightarrow \tau_f$=55.20 MPa)
Characteristic slip-weakening distance, d_0	0.4 m

[a] Accordingly to the results of Dunham (2007) we set the width of the fault so that the supershear transition can occur. From his Fig. 8 and considering a bounded fault a rough estimate of the minimum width to have supershear rupture propagation is given by $(0.8 L_{trans}^{(3-D)})/2 = 5.6$ km for our parameters.

[b] The spatial discretization ensures a good resolution of the breakdown zone length (X_b). On average we have: $<N_c> = <X_b>/\Delta x = 100$ (see Fig. 4d).

[c] For the adopted parameters the Courant–Friedrichs–Lewy ratio, $w_{CFL} = v_s \Delta t/\Delta x$, equals 0.083 and a conservative estimate (e.g., Archuleta and Frazier, 1978) of the critical frequency for spatial grid dispersion, $f_{acc}^{(s)} = v_s/(6\Delta x)$, equals 115 Hz. As required by explicit time stepping schemes we satisfy the condition $\Delta t \le \Delta x/(2 v_P)$.

(x_1^H, x_3^H) (the nucleation procedure is realized by initially forcing the rupture to expand at a constant rupture speed, as thoroughly described in Bizzarri, 2010) and then spreads bilaterally and spontaneously over the fault, obeying the linear slip-weakening (SW) friction (Ida, 1972). The depth of the hypocenter guarantees that the rupture accelerates to the supershear regime well before interacting the free surface ($x_3 = 0$), which is well-known to enhance the propensity for a supershear transition (e.g., Olsen et al., 1997; Bizzarri, 2010). The parameters adopted in the present study are reported in Table 1.

The slip-weakening constitutive model assumed here (see Eq. (25) in Bizzarri, 2011) prescribes that the fault shear traction linearly degrades with the increasing fault slip u from the upper yield stress τ_u (the finite material peak strength) down to the residual level τ_f. This traction drop is not abrupt, as in the Leonov–Panasyuk–Dugdale model (Leonov and Panasyuk, 1959), but it occurs over a characteristic length scale (the slip distance d_0) and thus over a finite time (the breakdown zone time, T_b; e.g., Bizzarri et al., 2001). It can be regarded as an extension of the interatomic cohesion model in brittle solids and it can be regarded as an idealization of more elaborated friction laws, accounting for the large number of chemical and physical processes that can potentially take place during faulting (Bizzarri, 2011). Indeed, at the microscale, lubricants, possible phase transitions and other mechanisms can play an important role in defining the above-mentioned levels of stress, as well as the transition between them. This friction law is able to capture the most significant features of a propagating rupture, as discussed in Bizzarri (2011).

In each node of the fault we compute the rupture speed v_r as the inverse of the slowness:

$$v_r(x_1, x_3) = \frac{1}{\| \nabla_{(x_1, x_3)} t_r(x_1, x_3) \|} \tag{1}$$

where x_1 and x_3 are the strike and depth directions, respectively, and the array t_r represents the rupture times, defined as the first time instant when the fault slip velocity, in that node, exceeds the

threshold value $v_l = 0.01$ m/s. We compute the spatial derivatives of t_r in Eq. (1) as it follows (e.g., Lapidus and Pinder, 1999):

$$\frac{\partial}{\partial x_1} t_r(x_1, x_3) =$$

$$\frac{1}{\Delta x} \frac{\tilde{t}_r(i+1, k+1) - \tilde{t}_r(i-1, k+1) + \tilde{t}_r(i+1, k-1) - \tilde{t}_r(i-1, k-1)}{4} \tag{2}$$

And

$$\frac{\partial}{\partial x_3} t_r(x_1, x_3) =$$

$$\frac{1}{\Delta x} \frac{\tilde{t}_r(i+1, k+1) - \tilde{t}_r(i+1, k-1) + \tilde{t}_r(i-1, k+1) - \tilde{t}_r(i-1, k-1)}{4} \tag{3}$$

where the symbol $\tilde{q}$ indicate the discrete equivalent of a generic quantity q the doublets (i,k) define a fault node located at the position $i\Delta x$ in the strike direction (x_1) and at the depth $(k-1)\Delta x$ (Δx being the spatial discretization in both x_1 and x_3 directions).

3. Numerical results for a 3-D rupture

In order to determine if the forbidden zone truly exists, as well as to understand its properties if it is not forbidden, and to better understand the supershear rupturing process, we carried out numerical calculations using finer grids than had ever been used before (5 m square grids). This extraordinary spatial resolution, associated with a time step of 1.2×10^{-4} s, gives an unprecedented resolution of the cohesive zone; on average we have $<N_c> = <X_b>/\Delta x = 100$ (see next Fig. 4d). For comparison, the best resolved model of Day et al. (2005) uses $<N_c> = 0.9$.

Fig. 1a shows the geometry of the problem and the adopted parameters are listed in Table 1. These parameters guarantee that the rupture will reach supershear speeds. Supplementary Movies 1 and 2 show the development of the cohesive zone and the change of the rake angle, respectively, as the rupture propagates.
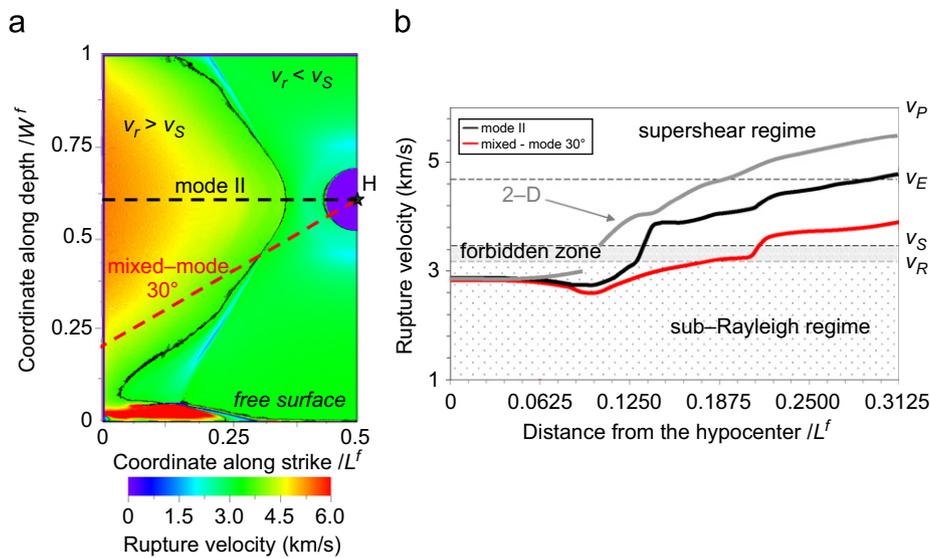
Fig. 2. (a) Distribution of the rupture speed on the left half of the fault plane. The purple region denotes the initial patch where nucleation occurs. The black line is the separation between regions experiencing sub- and super-shear rupture speeds. The lines along which the rupture velocities will be plotted in (b) are shown by red and black dashed lines. (b) Plot of the rupture velocity as a function of the hypocentral distance, along profiles shown in (a). The grey line reports the correspondent results for a 2–D, pure mode II spontaneous rupture. (For interpretation of the references to color in this figure legend, the reader is referred to the web version of this article.)
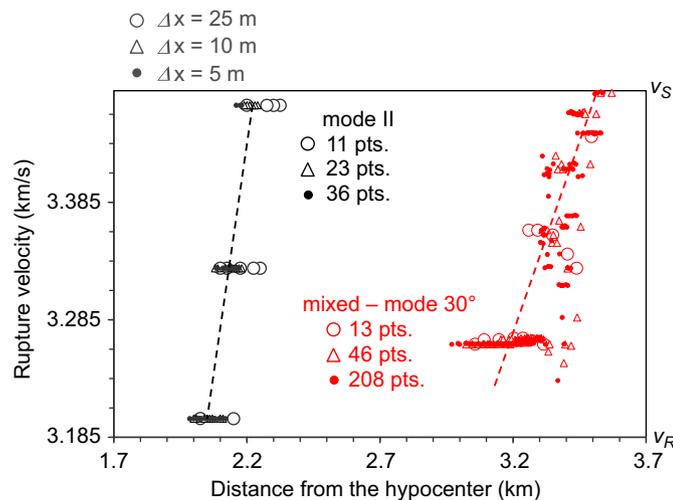

Fig. 3. Zoom of the forbidden zone. The number of points failing within the forbidden zone are also indicated for the different resolution of the models. The number of grid points lying within the forbidden zone are 36 and 208 for the pure mode II and the mixed mode case, respectively. Even with a rougher discretization of 25 m grid size, we have 11 and 13 points in this zone, respectively.

(The cohesive zone represents the region where the traction degrades from the upper yield level down the residual level.)

Supplementary material related to this article can be found online at doi:10.1016/j.epsl.2012.09.053.

Fig. 1b shows a snapshot of the fault slip at time $t = 1.92$ s. For comparison, we show the situation for the 2-D mode II case, carried out using a similar calculation method, in Fig. 1d. In 3-D, we see that unlike in the pure 2-D mode II case, the leading edge of the cohesive zone does not appear to have the jump in space once the rupture becomes supershear, as seen in Fig. 1d. (We recall here that the leading edge is the line which separates points of the fault plane which are at rest (i.e., having zero slip) from points which are already moving.) However, if we zoom-in to look at the details of the dashed zone of Fig. 1b, plotted in Fig. 1c, we

see a knee in the trailing edge (the locus of moving points where the slip equals the characteristic slip-weakening distance), which formally represents a weak jump in space for a given depth. (The trailing edge is the locus of moving points where the slip equals the characteristic slip-weakening distance.) For example, if we refer to the depth $x_3 = 0.9W^f$ (dashed white line in Fig. 1c) there is an interval along the strike direction ($x_1 \in]0.24L^f, 0.25L^f[$, thick red segment in Fig. 1c) where the fault points are at rest which is surrounded by two regions where the points are already moving ($x_1 \in [0.21L^f, 0.24L^f]$ and $x_1 \geq 0.25L^f$. The unbroken interval will disappear at the next time level, in that depth $x_3 = 0.9W^f$ all points with strike coordinate lower than the location of the trailing edge will be moving.

By looking at Fig. 1d we can see that the jump of the rupture (once the rupture becomes supershear) occurs at a distance of 1.86 km from the nucleation point. This formally defines $L_{trans}^{(2-D)}$, the distance at which the supershear transition occurs. This figure replicates what Andrews (1976) early found with a different and non-dimensional set of parameters (see his Fig. 3; see also Fig. 2a and d in Bizzarri et al., 2001 and Fig. 2a in Bizzarri and Cocco, 2005). Das and Aki (1977), by studying a transient mode II crack expansion in an infinite, isotropic, homogeneous, elastic solid subject to a remote shear stress, confirmed the numerical results of Andrews (1976), by adopting a critical stress criterion. The secondary, supershear rupture front is separated from the primary, sub-Rayleigh one by a region which has zero slip (i.e., an unbroken region).

In the 3-D case we can see that at a distance $L_{trans}^{(3-D)} = 2.17$ km from the hypocenter, the rupture becomes supershear (see Fig. 2a, where the black contour lines emphasize the region where v_r exceeds v_S). It is interesting to remark that, for the same parameters and the same nucleation procedure, our results predicts that $L_{trans}^{(3-D)} > L_{trans}^{(2-D)}$ (their ratio $L_{trans}^{(3-D)}/L_{trans}^{(2-D)}$ equals 1.12), in agreement with the conclusion of Dunham (2007). Indeed, by looking at his Fig. 5 and extrapolating, we have that for our parameters $L_{trans}^{(2-D)} \sim 12L_{fric}$ while $L_{trans}^{(3-D)} \sim 25L_{fric}$, where L_{fric} is a frictional length scale, which, for the linear SW model, can be set as $Gd_0/(\tau_u - \tau_f)$ or $Gd_0/(\tau_0 - \tau_f)$. It is important to remark that the comparison with the results by Dunham (2007) is only qualitative, in that his estimates reported above (for our
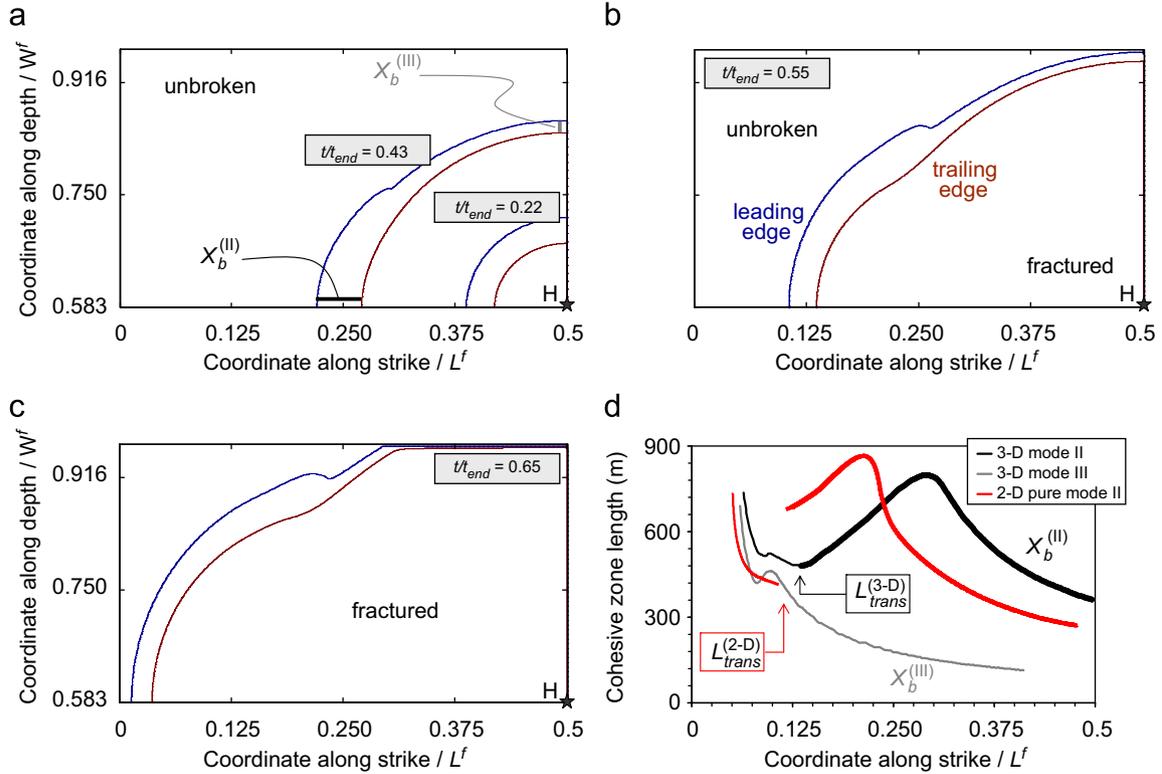
Fig. 4. (a)–(c) Snapshots of selected frames (from Supplementary Movie 2), showing the cohesive zone. The ratios of the times of snapshots over the total computational time are marked. (d) Width of the cohesive zone X_b as a function of distance from the hypocenter, along the pure inplane (mode II, black) and the pure antiplane (mode III, grey) directions of our fault. (For interpretation of the references to color in this figure, the reader is referred to the web version of this article.)

parameters: $L_{trans}^{(2-D)} = 6.5$ km and $L_{trans}^{(3-D)} = 14$ km, when $L_{fric} = Gd_0/(\tau_u - \tau_f) = 551$ m) refer to an unbounded fault.

4. Penetration of the Forbidden Zone

The most important results emerging from Fig. 1b is that there is no jump in the rupture velocity. This is more explicitly visible in Fig. 2a, where we plot the rupture speed distribution over the fault plane, and show regions which remained subshear and those which reached supershear speeds. In Fig. 2b, we plot the rupture speed along the pure mode II and a chosen mixed-mode direction. The rupture velocity clearly passes through the "forbidden zone" in both directions, the change in gradient of the curve on either side of the forbidden zone being particularly sharp for the mixed-mode case. Thus, though the crack front does pass through the forbidden zone, it passes through it fast, as it emerges from Fig. 3. Madariaga and Olsen (2000) did propose this idea, based on numerical simulations which did not have the same level of resolution, compared to those discussed in this paper. The penetration of the forbidden zone was also shown in Bizzarri and Cocco (2005); their Fig. 2c, but for a special non-dimensional set of parameters (that of Andrews, 1976). In the pure mode II direction, the rupture then passes through the Eshelby speed $\nu_E = 2^{1/2}\nu_S$ without any perceptible change of gradient and approaches ν_P. The expected increase of the values of the supershear rupture speeds near the free surface is very clearly seen (Olsen et al., 1997; Aagaard and Heaton, 2004; Bizzarri, 2010). However, we emphasize that in our simulations the penetration of the forbidden zone is not due to phase conversion along the free surface or to interactions with the stress field generated by the sliding near the free surface, as shown by Kaneko and Lapusta (2010; their Figs 7 and 9c).

In Fig. 3 we report a zoom of the forbidden zone $[\nu_R, \nu_S]$. In this plot we superimpose the results pertaining to three different numerical experiments, when we only vary the spatial and temporal discretization. It is apparent that the number of points failing within the forbidden zone increases as the resolution becomes finer. The number of points within $[\nu_R, \nu_S]$ is also marked in the figure. The discrete jumps in the rupture speed do not depend on the adopted numerical scheme (Eqs. (2) and (3)), which performs better than other methods we examined.

5. On the shrinking of the cohesive zone

Fig. 4(a–c) shows the snapshots, taken from Supplementary Movie 1, of the behavior of the evolution of the cohesive zone through time. In Fig. 4d we report the cohesive zone width in the mode II and mode III directions, plotted against the distance from the hypocenter. At the beginning of the rupture process, the cohesive zone has roughly the same width in both the directions. As rupture progresses from rest, the cohesive zone in the pure mode III direction continuously decreases, as the rupture accelerates to the shear wave velocity. When it reaches this limiting speed, the cohesive zone asymptotically reaches a final width. This is in contrast to the pure mode II direction, where the cohesive zone width at first decreases as the rupture accelerates, but then increases as its leading edge starts moving faster than the trailing edge, and moves into the supershear regime. The cohesive zone shape becomes much more complicated as rupture continues, and the shapes of the leading and trailing edges both change. As the trailing edge also starts moving faster, the cohesive zone width again starts decreasing. The time required for the stress to drop from the yield stress (τ_u) where rupture starts occurring to the final stress level (τ_f) at which the
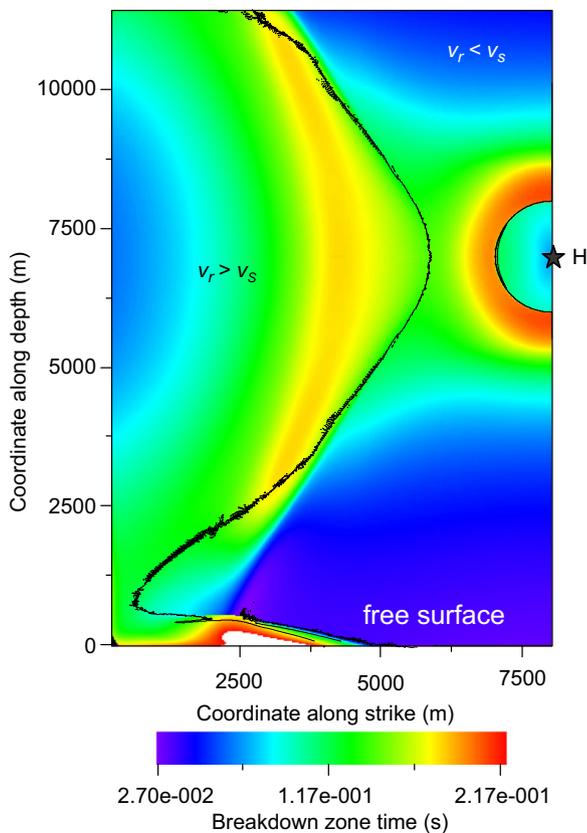
Fig. 5. Spatial distribution of the breakdown zone time T_b, determined as the difference, at each fault node, of the time when τ first reaches the residual level of friction τ_f and the time when τ first reaches the upper yield stress τ_u. As in Fig. 2a the black contour line emphasizes the region where the rupture is supershear. (For interpretation of the references to color in this figure, the reader is referred to the web version of this article.)

Fig. 6. Evolution of the energy rate F at the rupture tip as a function of the rupture speed. We compute F following Achenbach (1972) and generalizing its formulation valid for a 2-D singular crack to our 3-D case with a cohesive zone (see Eq. (4)). The computation has been done separately for the two profiles aligned along the mode II and mode III direction (reported here as black and pink lines, respectively). The thick part of the black line pertains to the supershear regime. Note that F assumes positive values in the forbidden zone. (For interpretation of the references to color in this figure legend, the reader is referred to the web version of this article.)

stress drop process is completed ("breakdown time"), is shown in Fig. 5.

The shrinking of the cohesive zone after the supershear transition is already known from the 2-D pure mode II results of Andrews (1976); for comparison, in Fig. 4d we plot in red the behavior of the corresponding 2-D rupture. Remarkably, the general shape of the cohesive zone in 2-D is quite similar to those obtained for the mode II of the 3-D simulation. The only difference is a spatial shift, which we expect from the knowledge of the transition lengths (also marked in Fig. 4d), which is lower in 2-D compared to 3-D (see Section 3). In 3-D the shrinking is more evident in the mode III direction than in the mode II; this makes sense, since the shrinking of the cohesive zone is intimately related to the increase of the peak fault slip velocity (Bizzarri et al., 2001, their equation (A5)), increase which in turn is more significant in the mode III direction (see Fig. A1 and A2 in Bizzarri, 2012). This is also in agreement with the theoretical prediction of Palmer and Rice (1973) pertaining to a nonspontaneous 2-D crack obeying a Barenblatt-type process region (namely, a linear position-weakening friction law, in which the traction degrades linearly with the position reached by the rupture tip, instead of with the cumulated slip).

The spatial distribution of breakdown zone time T_b is reported in Fig. 5, from which it is apparent that, in general, T_b varies depending on the position on the fault. In particular, it is clear that overall T_b is lower in the mode III direction with respect to the mode II direction. In the mode III direction the decrease of T_b is continuous, while in the mode II direction it initially decreases, once the rupture develops spontaneously outside the nucleation
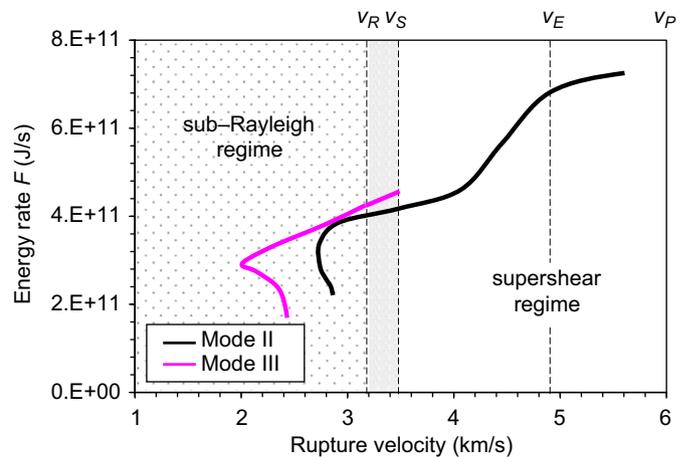
patch. When the supershear transition occurs (see the black contour in Fig. 5), T_b initially increases; this is visible from the yellow arc in Fig. 5. This increase of the cohesive zone in the mode II direction is due to the bird of the supershear front, which, contrarily to what happens in 2–D is not separated from the inner front. Moreover, this increase of T_b along the mode II direction is intimately connected to the increase of the cohesive zone length X_b occurring in the same direction (see Fig. 4d). We also emphasize that, once the sustained supershear speeds are attained by the rupture, then the cohesive zone starts to shrink markedly also in the mode II direction, just as observed for X_b.

6. Energy flux at the rupture tip

Since crack growth involves material separation, which is an energy consuming physical process, it requires a positive energy flux at the crack tip. More explicitly, the leading edge, which is responsible of the decohesion mechanism, requires that some energy is supplied from the surrounding stress field to the crack edge region (Achenbach, 1972). In Fig. 6 we plot the rate of work F as a function of the rupture speed in the modes II and III directions of our fault. The rate of work F is defined as it follows:

$$F(t) = \iint_{\Pi(t)} (\mathbf{T}(\xi,t) - \mathbf{T}_{res}(\xi)) \cdot v(\xi,t) d\xi$$
$$= \iint_{\Pi(t)} (\mathrm{T}_1(\xi_1,\xi_3 t) - \tau_f) v_1(\xi_1,\xi_3,t) + \mathrm{T}_3(\xi_1,\xi_3,t) v_3(\xi_1,\xi_3,t) d\xi_1 d\xi_3$$
(4)

where $\mathbf{T}$ and $\mathbf{T_{res}}$ are the fault shear traction vector and its residual level, respectively (τ and τ_{res} are their Euclidean norms, respectively), $\Pi(t)$ denotes a zone surrounding the crack tip and ξ maps the fault. In the framework of the Griffith's theory, the energy F extracted from the body containing the rupture is totally converted into the surface energy of the newly formed surfaces. Most remarkably, we see that F assumes positive values even in the forbidden zone in $[v_R, v_S]$ and its rate is also positive, contrary to the pure mode II calculations (Burridge et al., 1979; Broberg, 1999; see Fig. 1 of Das, 2010).

7. Conclusions

For more than 30 years, after the theoretical and numerical results pertaining to steady crack or 2-D, pure mode II ruptures, it has been assumed that an earthquake cannot propagate with a velocity within the so-called forbidden zone $[v_R, v_S]$ (Andrews, 1976; Burridge et al., 1979). In the present paper, we have performed numerical experiments of a 3-D rupture, with an unprecedented spatial and temporal resolution to explore whether this is really impossible.

Even for our simple 3-D configuration (homogeneous fault properties and linear slip-weakening friction law), the rupture speed does enter the forbidden zone $[v_R, v_S]$, in contrast to the 2-D pure mode II rupture. In the latter, we clearly observe a jump of the rupture front and after this the rupture speed is greater than the shear wave speed, with an unbroken region in between the sub-Rayleigh and supershear portions of the leading edge of the crack (Fig. 1d; see also Fig. 4d). Thus, we emphasize that though we did see a similar but very transient unbroken zone for the leading edge in 3-D (see Fig. 1c), there is no forbidden zone. We emphasize here that in the numerical simulations presented and discussed in the present paper the ratio of the cohesive zone length (X_b) to the radius of curvature of the rupture front at the supershear transition (namely, $L_{trans}^{(3-D)}$) is relatively high, so that the rupture is definitely far from satisfying the conditions for which the singular crack results of Richards (1976) are expected to be valid in the present case.

The presence of the knee in the 3-D case is also responsible of the two blue bands with low rupture speed, observed in Fig. 2a. These two bands form an angle of roughly 60° with respect to the mode II direction and emerge once the rupture begins to propagate at the supershear speed. Interestingly, these knees are the regions where the rake rotation most perceptible (see Supplementary Movie 2), with regions of positive and negative rake rotation located in contiguous regions. Though small (the maximum variation with respect to the initial direction is at most $\pm 15°$), the rake variation is significant once the rupture becomes supershear and it is maximum in the region near the knee of the rupture tip. Our simulations also show that the energy flux is always positive and it assumes positive values even in the forbidden zone, contrary to 2-D steady state solutions.

In summary, the result from 2-D calculations that strike-slip earthquakes cannot propagate at speeds between the Rayleigh and shear wave speeds does not hold for realistic 3-D faults, showing that 2-D results cannot simply be extended to the 3-D case. As pointed out by Dmowska and Rice (1986) the only possible special case in which a 3-D crack can be somehow describable by using a 2-D solution is when the cohesive zone is small compared to the radius of curvature of a tridimensional rupture front. This reflects in two possibilities, the first being that the transition occurs in a very late stage of the rupture and very far from the hypocenter when the curvature is very small and the second being that the cohesive zone is extremely small at the supershear transition. Both of these possibilities introduces serious problems, because it is very difficult, even with the present computational resources, have sufficiently good resolution of the cohesive zone at huge distance from the nucleation patch, due to the continuous contraction of the cohesive zone itself. On the other hand, having a very small cohesive zone compared to the transitional distance, automatically poses the problem of the correct resolution.

Our results have important implications for seismologists interpreting seismograms to infer details of the earthquake source process, and for earthquake engineers considering the generation of damaging waves from earthquakes in order to construct earthquake-resistant structures.

Appendix A. Supporting information

Supplementary data associated with this article can be found in the online version at http://dx.doi.org/10.1016/j.epsl.2012.09.053.

References

Aagaard, B.T., Heaton, T.H., 2004. Near-source ground motions from simulations of sustained intersonic and supersonic fault ruptures. Bull. Seismol. Soc. Am. 94 (6), 2064–2078, http://dx.doi.org/10.1785/0120030249.
Achenbach, J.D., 1972. in: Nemat–Nasser, S. (Ed.), Mechanics Today, vol. 1. Pergamon Press, NewYork. (chapter 1).
Andrews, D.J., 1976. Rupture velocity of plane strain shear cracks. J. Geophys. Res. 81, 5679–5687.
Andrews, D.J., 1994. Dynamic growth of mixed-mode shear cracks. Bull. Seismol. Soc. Am. 84 (4), 1184–1198.
Archuleta, R.J., Frazier, G.A., 1978. 3-D numerical simulations of dynamic faulting in a half space. Bull. Seism. Soc. Am. 68, 573–598.
Ben-Menhahem, A., Toksöz, N., 1963. Source mechanism from spectrums of long-period surface waves. 2. The Kamchatka earthquake of November 4, 1952. J. Geophys. Res. 68, 5207–5222.
Benioff, H., Press, F., Smith, S., 1961. Excitation of the free oscillations of the Earth by earthquakes. J. Geophys. Res. 66, 605–619.
Bernard, P., Baumont, D., 2005. Shear Mach wave characterization for kinematic fault rupture models with constant super-shear rupture velocity. Geophys. J. Int. 162, 431–447.
Bizzarri, A., 2009. Can flash heating of asperity contacts prevent melting? Geophys. Res. Lett. 36, L11304, http://dx.doi.org/10.1029/2009GL037335.
Bizzarri, A., 2010. How to promote earthquake ruptures: different nucleation strategies in a dynamic model with slip-weakening friction. Bull. Seism. Soc. Am. 100 (3), 923–940, http://dx.doi.org/10.1785/0120090179.
Bizzarri, A., 2011. On the deterministic description of earthquakes. Rev. Geophys. 49, RG3002.
Bizzarri, A., 2012. Rupture speed and slip velocity: what can we learn from simulated earthquakes? Earth Planet. Sci. Lett. 317–318, 196–203.
Bizzarri, A., Cocco, M., 2005. 3D dynamic simulations of spontaneous rupture propagation governed by different constitutive laws with rake rotation allowed. Ann. Geophys. 48 (2), 279–299.
Bizzarri, A., Cocco, M., Andrews, D.J., Boschi, E., 2001. Solving the dynamic rupture problem with different numerical approaches and constitutive laws. Geophys. J. Int. 144, 656–678.
Bizzarri, A., Dunham, E.M., Spudich, P., 2010. Coherence of Mach fronts during heterogeneous supershear earthquake rupture propagation: Simulations and comparison with observations. J. Geophys. Res. 115, B08301, http://dx.doi.org/10.1029/2009JB006819.
Bouchon, M., Bouin, M.-P., Karabulut, H., Toksöz, M.N., Dietrich, M., Rosakis, A.J., 2001. How fast is rupture during an earthquake? New insights from the 1999 Turkey earthquakes. Geophys. Res. Lett. 28, 2723–3016.
Broberg, K.B., 1999. Cracks and Fracture. Academic Press, New York.
Burridge, R., 1973. Admissible speeds for plane-strain self-similar shear cracks with friction but lacking cohesion. Geophys. J. R. Astron. Soc. 34, 439–455.
Burridge, R., Conn, G., Freund, L.B., 1979. The stability of a rapid Mode II shear crack with finite cohesive traction. J. Geophys. Res. 84, 2210–2222.
Das, S., Aki, K., 1977. A numerical study of two-dimensional spontaneous rupture propagation. Geophys. J. Roy. Astr. Soc. 50, 643–668.
Das, S., 2010. Earthquake supershear rupture speeds. Tectonophysics 493, 213–215, http://dx.doi.org/10.1016/j.tecto.2010.07.009.
Day, S.M., Dalguer, L.A., Lapusta, N., Liu, Y., 2005. Comparison of finite difference and boundary integral solutions to three-dimensional spontaneous rupture. J. Geophys. Res. 110, B12307, http://dx.doi.org/10.1029/2005JB003813.
Dmowska, R., Rice, J.R., 1986. Fracture theory and its seismological application. in: Teisseyre, R. (Ed.), Continuum Theories in Solid Earth Physics of Series Physics and Evolution of the Earth's Interior, 3. Elsevier and Polish Scientific Publishers, pp. 187–255.
Dunham, E.M., 2007. Conditions governing the occurrence of supershear ruptures under slip-weakening friction. J. Geophys. Res. 112, B07302.
Dunham, E.M., Archuleta, J.R., 2005. Near-source ground motion from steady state dynamic rupture pulses. Geophys. Res. Lett. 32, L03302.
Gutenberg, B., 1995. Magnitude determination for larger Kern County shocks, 1952: effects of station azimuth and calculation methods. In: Earthquakes in Kern County, California during 1952, Bull. 171, US Division of Mines.
Ida, Y., 1972. Cohesive force across the tip of a longitudinal shear crack and Griffith's specific surface energy. J. Geophys. Res. 77, 3796–3805.

Kaneko, Y., Lapusta, N., 2010. Supershear transition due to a free surface in 3-D simulations of spontaneous dynamic rupture on vertical strike-slip faults. Tectonophysics 493 (3–4), 272–284, http://dx.doi.org/10.1016/j.tecto.2010.06.015.

Lapidus, L., Pinder, G.F., 1999. Numerical Solution of Partial Differential Equations in Science and Engineering. Wiley, New York.

Leonov, M.Ya., Panasyuk, V.V., 1959. Development of the finest cracks in a solid body. Prikl. Mekh. 5, 391–401.

Madariaga, R., 1983. High frequency radiation from dynamic earthquake fault models. Ann. Geophys. 1, 17–23.

Madariaga, R., Olsen, K.B., 2000. Criticality of rupture dynamics in 3-D. Pure Appl. Geophys. 157, 1891–2001.

Olsen, K.B., Madariaga, R., Archuleta, R.J., 1997. Three-dimensional dynamic simulation of the 1992 Landers earthquake. Science 278, 834–838.

Palmer, A.C., Rice, J.R., 1973. The growth of slip surfaces in the progressive failure of over-consolidated clay. Proc. R. Soc. London Ser. A 332, 527–548.

Richards, P.G., 1976. Dynamic motions near an earthquake fault: a three-dimensional solution. Bull. Seismol. Soc. Am. 66 (1), 1–32.

Robinson, D.P., Brough, C., Das, S., 2006. The Mw 7.8, 2001 Kunlunshan earthquake: Extreme rupture speed variability and effect of fault geometry. J. Geophys. Res. 111, B08303.

Rosakis, A.J., Samudrala, O., Coker, D., 1999. Cracks faster than the shear-wave speed. Science 284, 1337–1340.